Available online at www.sciencedirect.com
ScienceDirect
Polymer 47 (2006) 6698–6709
polymer
www.elsevier.com/locate/polymer

Synthesis of imidazolium salts and their application in epoxy montmorillonite nanocomposites

J. Langat [a], S. Bellayer [b,1], P. Hudrlik [a], A. Hudrlik [a], P.H. Maupin [c], J.W. Gilman Sr. [b], D. Raghavan [a,*]

[a] *Department of Chemistry, Howard University, 525 College Street, NW, Washington, DC 20059, USA*
[b] *Fire Research Division, National Institute of Standards and Technology, Gaithersburg, MD 20899, USA*
[c] *Office of Basic Energy Science, Office of Science, U.S. Department of Energy, Washington, DC 20585, USA*

Received 10 February 2006; received in revised form 27 June 2006; accepted 28 June 2006
Available online 9 August 2006

Abstract

Considerable research has been conducted in improving the performance characteristics of nanocomposites, however, relatively few attempts have been made to address the thermal stability of nanocomposites. An attempt is being made to improve the thermal properties of nanocomposites by synthesizing imidazolium salts from 2-methyl imidazole and ion exchanging the salts with clay minerals. This study focuses on the role of the chemistry of imidazolium salt(s) used in functionalizing clay and processing conditions in the formulation of epoxy nanocomposites. The nanodispersion of clay in an epoxy matrix is evaluated qualitatively by X-ray diffraction (XRD), transmission electronic microscopy (TEM), and laser scanning confocal microscopy (LSCM). We demonstrate the use of LCSM for quantitative image analysis and to study the dispersion of clay layers, tagged with a fluorescent dye in the epoxy matrix. XRD and TEM results reveal that the hand mixed nanocomposite has tactoid morphology, while ultrasonicated organoclay (without hydroxyl group) epoxy nanocomposite exhibits a mixed morphology, and an ultrasonicated organoclay (with hydroxyl group) epoxy nanocomposite had well dispersed clay distribution in the epoxy matrix. Results from the three complimentary techniques enable the characterization of the clay platelets over several length scales ranging from the micrometer to the nanometer scale.

Keywords: Clay nanocomposites; Thermal stability; Confocal microscopy

1. Introduction

During the last decade, the area of nanoclay filled polymers has received much attention from both the scientific and technological communities with the expectation that the materials designed will be lighter and more superior to the pristine polymers. In particular, the attractiveness of polymer–clay nanocomposites resides in the potential of adding small amounts of clay platelets to polymeric resin, to dramatically improve mechanical, thermal, barrier, and flame-retardant properties [1–10]. Because of the potential benefits of adding inexpensive clay filler to the polymer matrix, the automotive and aerospace industries view polymer–clay hybrid nanocomposites as promising structural materials for the 21st century [11].

Considerable research has been conducted to study the structure–property relationship of organically modified clay–epoxy nanocomposites [12–18]. Tsai and Sun [19] modeled the load transfer efficiency in nanocomposites and noted that significant enhancement in reinforcement can be achieved by having the clay platelets well dispersed in the polymer matrix. By ion exchanging Na^+, Ca^{2+}, or K^+ on the clay surface with a long chain cation, attempts have been made to disperse layered particles (hydrophilic) in polymer matrix (hydrophobic). Typically nanoclays treated with alkyl ammonium ions have been used to produce clay–epoxy nanocomposites. The architecture of the alkyl ammonium ion has been commonly chosen

* Corresponding author. Tel.: +1 202 806 4427; fax: +1 202 806 5442.
E-mail address: draghavan@howard.edu (D. Raghavan).
[1] Guest Researcher from France.

0032-3861/$ - see front matter © 2006 Elsevier Ltd. All rights reserved.
doi:10.1016/j.polymer.2006.06.067

so as to improve clay compatibility with a given polymer resin and provide sufficient layer separation for polymer chains to infiltrate. Recently, Brown et al. [20] investigated the ability of secondary functional groups on the alkyl ammonium cations to promote intra-layer polymerization and clay exfoliation. The study found that the presence of hydroxyl groups in the bis(2-hydroxy-ethyl) methyl tallow ammonium cation facilitated clay exfoliation in a diglycidyl ether bisphenol A (DGEBA)/poly(ether amine) epoxy resin. This work clearly demonstrated the desirability of using onium salts having a secondary functional hydroxyl group for clay platelet exfoliation in epoxy matrix. Organic modifiers can participate in the reaction(s) with resin components and improve the miscibility of the clay with resin. Conceptually, the organic modifiers can assist in polymer network formation, interface reaction and ultimately dictate the final morphology of nanocomposite by providing layer separation.

Another approach to achieve clay platelet dispersion in polymer matrices is to add intercalating aid to enhance the compatibility between polymer and an organoclay [21–23]. An intercalating aid containing polar groups can be intercalated between the layers of the clay via strong hydrogen bonding. The intercalating aid weakens the ionic interaction between clay layers. Examples of intercalating aids are maleic anhydride, glycidyl methacrylate, and styrene. The selection criteria for choosing swelling agent/intercalating aid are based on its miscibility with the polymer and its ability to swell the organically modified clay.

The clay platelet morphology in a polymer matrix can also be altered based on the processing conditions. While there are reports that explore the importance of processing conditions to make exfoliated nanocomposite with thermoplastic matrix, limited work has been done to investigate the importance of processing parameters on exfoliated nanocomposite with thermoset matrix. Mechanical mixing (compounding, sonication, shear) is necessary – and the efficiency of mixing is dependent on the medium's viscosity and reactivity. Sonication of premixed nanoclay/polymer samples has been shown to be a promising technique in the dispersion or exfoliation of the nanoclay platelets in vinyl ester matrix [24]. All these approaches are attractive, and they provide a framework to manipulate the morphology of nanocomposites so as to achieve optimal properties.

Although factors influencing the morphology of nanocomposites have been studied, little is known about the long term thermal stability of nanocomposites [25,26]. This property becomes particularly relevant since most of the composite materials used in aerospace applications are exposed to elevated temperature for prolonged periods. To date, the thermal stability of epoxy nanocomposites has only been investigated for certain epoxy resins. These studies have reported an improvement in thermal stability of polymeric resin with the addition of layered silicate [27,28]. The mechanism of the improvement of thermal stability in polymer nanocomposites, however, is not fully understood. It is widely believed that at high temperature the amine grafted organic polymer layer will degrade from the clay particle surface resulting in more hydrophilic and less compatible clay aggregates dispersed in epoxy resin [13].

Thermogravimetric analysis (TGA)–MS studies of organo layered silicate showed that the onset temperature for decomposition of organic modifier can range from 150 °C to 220 °C [29,30]. If the organically modified clay filled nanocomposites are exposed to temperatures exceeding the decomposition temperature of organic modifier, the ammonium ions are capable of undergoing thermal dissociation to generate primary amines and protons. These protons can subsequently participate in the homopolymerization of epoxies [31]. The free amines can possibly react with the epoxide functionalities present inside the galleries or may diffuse out of clay particles and react with the epoxide functionalities in the bulk epoxy [32]. Because these amines are primary amines, the epoxy–primary amine reactions will yield only linearly cured epoxy chains unlike the conventional three dimensionally cured epoxy resin. Furthermore, the epoxy–primary amine reactions can create a stoichiometric imbalance and result in the plasticization of the epoxy networks because of excess primary amine [13]. Finally, the release of organic modifier from layered silicate at elevated temperature can have strong implications on the distribution of nanoclay platelets, interfacial properties, and on the ultimate mechanical properties of nanocomposite. Thus, the success of high performance nanocomposites depends on the stability of organic modifier used in the functionalization of clay as the organic treatment is the interface between layered silicate and polymer. A poor interface between polymer and layered silicate will often result in a microcomposite, or in a traditional filled system.

An approach to increase the onset of degradation temperature of the organoclay from 200–300 °C to >300 °C is to use synthetic clays instead of smectite clay, because the preparative chemistry for synthetic clay is relatively straightforward. For example, the surface of alpha-zirconium phosphate (α-ZrP) nanomaterials can be easily modified by various charge-carrying ionic polymers to achieve compatibilization and exfoliation of α-ZrP in various polymer matrices [33]. Synthetic clay has the distinct advantage of better control over the overall composition of layered material than natural clay composition and therefore lesser possibility of inconsistency in the nanocomposite result. It should be mentioned that synthetic clays are significantly more expensive than natural clays, so there are some hurdles that must be overcome for synthetic clay to be used in a commercial product.

Alternatively, the thermal stability of organically modified montmorillonite clay can be improved by selecting appropriate organic modifiers [34–41]. Severe et al. [34] found that the phosphonium exchanged montmorillonite provided better thermal stability than ammonium exchanged clays. A better understanding of the thermal behavior of phosphonium salts and their functionalized clay has been explained in detail by Xie et al. [41]. Like phosphonium salts, imidazolium salts have been used to improve the thermal stability of functionalized clay because the thermal stability of the imidazolium salt can be improved based on the substituents at various positions on the imidazole ring, counter ion, alkyl chain length, and

isomeric structure of the alkyl side group, etc. [37,38]. At present there has been only a handful of work performed to assess the potential of using the imidazolium molten salts as a replacement for the conventional alkyl ammonium surfactant on the formation of nanocomposites [35,36,39,42–44].

The scope of the present study is two-fold. The first section is dedicated to the synthesis of reactive imidazolium salt from 2-methyl imidazole, 1-bromohexadecane and chloroalcohols. In the past, short chain hydroxyalkyl imidazolium chlorides have been used for improving the performance of tetrafunctional epoxy resin because the hydroxyl group in the imidazolium salt can catalyze the polymerization occurring in the gallery space between the silicate layers [44]. The influence of long chain hydroxyalkyl imidazolium chlorides on the meso and nanoscale morphologies of clay platelets of the epoxy matrix is the subject of the study. The imidazolium salt modified montmorillonite clay is characterized with wide-angle X-ray scattering (WAXS) and thermal gravimetric analysis (TGA). The second part of the paper deals with the meso and nanoscale characterizations of the dispersion of imidazolium salt modified montmorillonite clay in epoxy resin. The mesoscale characterization of clay platelets in epoxy matrix is based on using the cationic-dye modified organo-MMT combined with laser scanning confocal microscope [39,40]. Results from wide-angle X-ray diffraction (WAXD) and transmission electron microscopy (TEM) measurements of nanocomposites are used to assist in the interpretation of the confocal results for the nanocomposites.

2. Experimental methodology[2]

2.1. Materials and general procedure

The 2-methyl imidazole, 1-bromohexadecane, 10-chlorodecanol, and Nile Blue A perchlorate were procured from Aldrich Chemical Company.[2] Sodium bicarbonate, THF, acetonitrile, sodium hydride, and petroleum ether were purchased from Fisher Scientific. Anhydrous THF was distilled from sodium and benzophenone just prior to use, while anhydrous acetonitrile was distilled from calcium hydride.

All reactions were carried out under a nitrogen atmosphere and transfers of non-aqueous liquids were carried out with nitrogen-flushed syringes. ^{1}H nuclear magnetic resonance (NMR) data were obtained with a General Electric 300 MHz NMR spectrometer and Bruker Avance 400 MHz NMR. Deuterated chloroform was used as the solvent and methylene chloride (5.30 ppm) served as internal reference in performing NMR experiments for all the samples.

2.2. Synthesis of imidazolium salts

Fig. 1 provides the reaction sequences used in the synthesis of 1-hexadecyl-2-methyl imidazole and 1-hexadecyl-3-(10-hydroxydecyl)-2-methylimidazolium chloride (HDHDMIM) from 2-methyl imidazole.

2.2.1. Synthesis of 1-hexadecyl-2-methyl imidazole

In a dry three-necked 50 mL round bottom flask equipped with a magnetic stir bar, 2.34 g of sodium hydride (60% dispersion in mineral oil, 0.06 mol) was weighed, and the flask was placed on a nitrogen line. To remove the mineral oil, the mixture was washed three times with 10 mL of petroleum ether (under nitrogen). 2-Methyl imidazole (5.06 g (0.06 mol)) and 10 mL of dry THF were gradually added into the flask containing the mixture and stirred for 1 h. 1-Bromohexadecane (9.30 mL (0.03 mol)) was added into the flask and the resulting mixture was stirred for 24 h at room temperature. After 24 h, unreacted sodium hydride was decomposed by adding 10 mL of saturated aqueous $NaHCO_3$ solution. To avoid any vigorous reaction, the $NaHCO_3$ solution was gradually added to the mixture in the flask for over 30 min. The resulting solution was then transferred into 125 mL separatory funnel and an

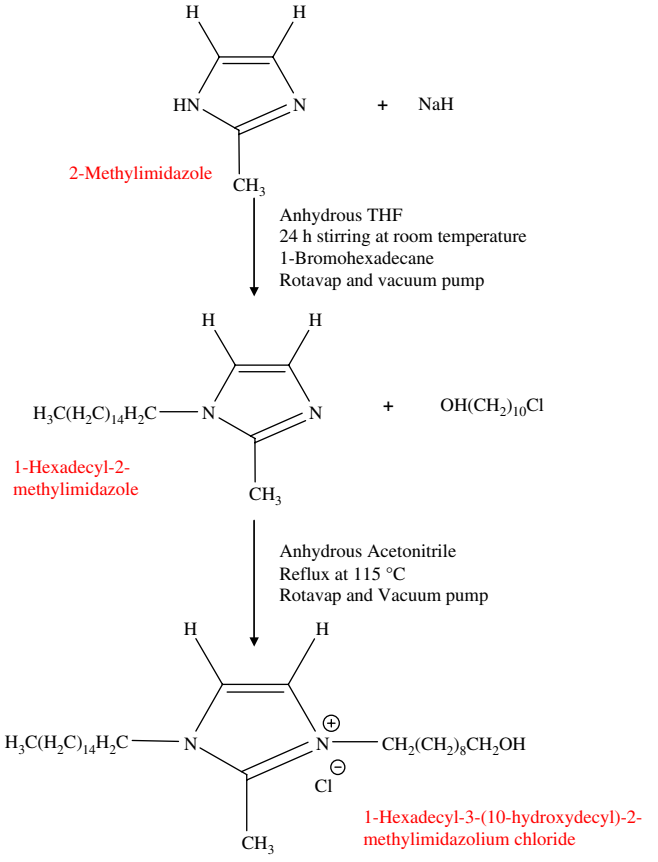

Fig. 1. Reaction scheme for synthesizing 1-hexadecyl-2-methyl imidazole and 1-hexadecyl-3-(10-hydroxydecyl)-2-methylimidazolium chloride from 2-methyl imidazole.

[2] This work was carried out by the National Institute of Standards and Technology (NIST), an agency of the U.S. government and by statute is not subject to copyright in the United States. Certain commercial equipment, instruments, materials or companies are identified in this paper in order to adequately specify the experimental procedure. This in no way implies endorsement or recommendation by NIST. The policy of NIST is to use metric units of measurement in all publications, and to provide statements of uncertainty or all original measurements. In this document, however, data from organizations outside NIST are shown, which may include measurements in non-metric units or measurements without uncertainty statements.

additional 60 mL of $NaHCO_3$ solution was added. The solution was extracted three times with petroleum ether and the petroleum ether extracted layers were combined and dried overnight using anhydrous magnesium sulfate. The mixture was filtered and the filtrate was collected. The filtrate was concentrated by rotary evaporation to obtain a solid product. The product was characterized by ^{1}H NMR and MALDI-TOF MS. The reaction was repeated several times and the yield of the product was found to be 95%. While some of the product was protonated with HCl to form 1-hexadecyl-2-methylimidazolium chloride (HDMIM), the remaining product was used for the synthesis of 1-hexadecyl-3-(10-hydroxydecyl)-2-methylimidazolium chloride (HDHDMIM).

2.2.2. Synthesis of 1-hexadecyl-2-methylimidazolium chloride (HDMIM)

In a dry three-necked 50 mL round bottom flask, 1-hexadecyl-2-methyl imidazole (0.25 g (0.814 mmol)) was dissolved in 7.5 mL ether by stirring for 30 min. 1.7 mL of 0.5 M HCl was added gradually to a stirring mixture. Upon completion of addition of HCl to the mixture, the entire mixture was stirred for an additional 3 h. The solid was recovered by stripping ether from the mixture using vacuum oven (room temperature). The yield of the product was found to be 95%. The product was characterized by MALDI-TOF MS and ^{1}H NMR. Table 1a summarizes the MALDI-TOF MS data of the final compound (HDMIM).

2.2.3. Synthesis of 1-hexadecyl-3-(10-hydroxydecyl)-2-methylimidazolium chloride (HDHDMIM)

To a 50-mL three-necked round bottom flask equipped with a condenser and a magnetic stir bar, 1-hexadecyl-2-methyl imidazole (0.912 g (0.003 mol)) was added. The flask was placed on a nitrogen line before adding 10 mL of anhydrous acetonitrile. 10-Chloro-1-decanol (0.61 mL (0.003 mol)) was added dropwise and the mixture was refluxed with continuous stirring at 115 °C. The reaction kinetics were followed by removing aliquots from the vessel at predetermined time intervals for a period of 3 weeks. The crude product was analyzed by ^{1}H NMR. The final mixture was transferred to a 125 mL separatory funnel and extracted three times with petroleum ether. The sample was concentrated through rotary evaporation of the petroleum ether extract. The compound was then further purified by redissolving in 1 mL of water, followed by extraction with petroleum ether. The water extract and petroleum ether extract were concentrated through rotary distillation. The concentrated water extract was dried further by pumping for 3 h at a pressure of 0.05 mm Hg. The compound (HDHDMIM) was characterized by ^{1}H NMR and MALDI-TOF MS. Table 1b summarizes the MALDI-TOF MS data of the final compound (HDHDMIM). The reaction was repeated several times and the yield of the final product was found to be $60 \pm 5\%$.

Table 1
MALDI-TOF MS data

Mass (*m*/*z*)	Compound
(a) 1-Hexadecyl-2-methylimidazolium chloride	
307.52	1-Hexadecyl-2-methylimidazolium chloride (s)
531.83	Dialkylated 1-hexadecyl-2-methylimidazolium chloride (w)
974.48	*meso*-Tetrakis(pentafluorophenyl)porphyrin (F20TPP) (m)
(b) 1-Hexadecyl-3-(10-hydroxydecyl)-2-methylimidazolium chloride	
190.15	Alpha cyano-4-hydroxycinnamic acid (matrix) (m)
307.57	1-Hexadecyl-2-methylimidazolium chloride
463.73	1-Hexadecyl-3-(10-hydroxydecyl)-2-methylimidazolium chloride (s)
531.9	Dialkylated 1-hexadecyl-2-methyl imidazole

s-Strong, m-medium, and w-weak.

2.3. Preparation of imidazolium functionalized clay

Na-Cloisite (Na-montmorillonite (Na^+-MMT) Southern Clay Products) has a cation exchange capacity (CEC) value of 92.6 mmol/100 g clay [43]. Using standard cation exchange techniques NaMMT was treated with Nile Blue A and a high temperature stable imidazolium-based cation, in a mass fraction ratio of 20:1 (imidazolium:Nile Blue A). Briefly, an appropriate amount of the optical probe and HDHDMIM salt necessary to achieve complete exchange was dissolved in 50 mL of hot ethanol–water mixture. NaMMT (5 g) was added with rapid stirring until the solid was well dispersed. The volume was adjusted to 100 mL with distilled water then stirred and heated for 5 h at about 70 °C. The exchanged clay was filtered, washed with hot 50% ethanol–water mixture, followed by 95% ethanol, until the filtrate was colorless. The washing was continued until the filtrate showed no chloride ions by checking the filtrate with 0.1 N $AgNO_3$ solution. The resulting clay was dried at 100 °C in a forced convection oven overnight and pulverized into fine powder. The clay with HDMIM was made by following a procedure similar to that described above. The purified organo-dyed-MMT clay, designated NB-HDHDMIM-MMT and NB-HDMIM-MMT, was characterized by X-ray diffraction (XRD) and thermal gravimetric analysis (TGA).

2.4. Thermogravimetric analysis and XRD analysis

Thermogravimetric analysis (TGA) was conducted using a Perkin Elmer 7 Series system under a nitrogen atmosphere. The thermogram was generated by placing 25 mg of the sample in a crucible and heating it from 30 °C to 600 °C at 20 °C/min. Nitrogen gas was allowed to flow at a rate of 40 mL/min. The standard uncertainty of the sample mass measurement was ±1%.

XRD analyses of the organoclay were performed using a Scintag Inc. XRG 3000 diffractometer with CuKα radiation (40 kV, 35 mA). The scanning speed and the step size were 0.01°/min and 0.04°, respectively.

2.5. Epoxy nanocomposites

Two different organoclays were added to the epoxy resin and mixed using two different processing conditions to form nanocomposite specimens. The mixing conditions used for preparing nanocomposite samples were hand mixing and ultrasonication. For preparing epoxy nanocomposite specimens by ultrasonication, organo-dyed-MMT clay (0.3 g) was initially

soaked in glycidyl methyl acrylate (1.5 g), while epoxy resin (5 g) was separately soaked in glycidyl methyl acrylate (1 g) for 24 h. After soaking the clay and resin in glycidyl methyl acrylate, both clay and resin were combined and sonicated using a high power VWR Branson Ultrasonifier 250 R (frequency of 20 kHz) at 40% duty cycle and at different output controls (from 1 to 10) for 30 min. During ultrasonication, the temperature of the mixture was maintained below 35 °C by placing the reaction vessel in an ice jacket. To the sonicated mixture, 1.1 g of *meta*-phenylene diamine (MPDA) at 60 °C was added and thoroughly mixed. The curative added mixture was poured into a silicone mold and cured at 80 °C for 2 h and post-cured at 110 °C for 7 h in a Lab-Line Instrumentation programmable vacuum oven. The other epoxy nanocomposite specimen was prepared by hand mixing Nile Blue clay, resin, glycidyl methacrylate (GMA), and MPDA followed by a similar curing cycle.

2.6. XRD and TEM analyses of epoxy nanocomposites

The nanocomposite dog-bone produced during the molding process has a fairly smooth surface. The dog-bone specimens were cut to size and analyzed by XRD using a Scintag Inc. XRG 3000 diffractometer.

TEM specimens were cut from dog-bones using a Leica ultramicrotome, equipped with a diamond knife. They were collected on the surface of a water-filled trough and lifted from the surface using 200 mesh copper grids. Electron micrographs were taken with a Philips EM400T at an accelerating voltage of 120 kV.

2.7. Confocal microscopy of epoxy nanocomposites

The nanocomposite sample was characterized using an upright laser scanning confocal microscope (Zeiss LSM 510). The dye doped organoclay filled epoxy samples were excited at 488 nm using Ar^+ laser light; fluorescence light emitted (560–615 nm) from the sample was detected with a photomultiplier tube. The 20× objective was used to give a 460 μm × 460 μm field of view and focal plane resolution depth of 1 μm. Images were acquired by focusing the laser beam beneath the surface of the sample at 1 μm interval. Several images at each location along the depth of the cured film were obtained. The image acquisition time was 30 s per position. The images were collected for the entire sample in few hours and this allowed for the reconstruction of the clay distribution in the bulk matrix.

3. Results and discussion

N-Alkylated imidazoles and *N*,*N*-dialkylated imidazolium salts have been prepared by various alkylation strategies [45–47]. Here we report the synthesis and characterization of a dialkylated imidazolium salt from 2-methyl imidazole having a hydroxyl group at the terminal end of one of the alkyl chains.

Fig. 2 is the NMR spectra of 2-methyl imidazole, 1-hexadecyl-2-methyl imidazole and 1-hexadecyl-3-(10-hydroxydecyl)-2-methylimidazolium chloride. The ^{1}H NMR spectrum of 2-methyl imidazole has a peak at a chemical shift of 7.0 ppm, which is characteristic of the proton associated with the olefinic carbon in the starting compound. The protons associated with the olefinic carbon are not easily distinguishable, as noticed by the peak integration value. It is reasonable to assume that the proton peaks appear as a single peak because of the fast chemical exchange of the NH proton between the N atoms in imidazole [48]. We notice in the NMR spectrum of the alkylated compound, the disappearance of the peak (at 2.2 ppm) corresponding to the proton associated with the N atom of 2-methyl imidazole. Further evidence for the conversion of 2-methyl imidazole to hexadecyl 2-methyl imidazole is the appearance of twin olefinic proton peaks at 6.9 ppm and 6.8 ppm. They appear as two peaks because the environment of the olefinic proton is not similar to that observed in 2-methyl imidazole. A peak at 3.8 ppm is observed that corresponds to the methylene protons adjacent to the N atom of 1-hexadecyl-2-methyl imidazole. Detailed assignment of the NMR peaks can be found in Fig. 2. As expected, many of the ^{1}H NMR peaks in the protonated sample of 1-hexadecyl-2-methylimidazolium chloride appear downfield relative to the nonprotonated sample (data available but not included).

The MALDI-TOF MS spectrum of 1-hexadecyl-2-methylimidazolium chloride shows an intense peak at 307.54 (Table 1a). This corresponds to the molecular mass of the protonated form of 1-hexadecyl-2-methylimidazolium ion. Also a weak peak at *m*/*z* 531 corresponding to the dialkylated compound ion was observed in the spectrum.

In the next step, 1-hexadecyl-2-methyl imidazole was converted to 1-hexadecyl-3-(10-hydroxydecyl)-2-methylimidazolium chloride. The peak at ~2.5 ppm is assigned to the hydroxyl proton in the 1-hexadecyl-3-(10-hydroxydecyl)-2-methylimidazolium chloride. The methylene proton peak observed at 3.8 ppm in the ^{1}H NMR spectra of 1-hexadecyl-2-methyl imidazole is observed in the final compound at 4.2 ppm. Another methylene proton peak neighboring to the OH atom is observed at 3.5 ppm. All of the assignments are given in Fig. 2d, and were obtained using correlations from a DQF-COSY experiment. The MALDI data of the final compound also showed the desired ion peak at *m*/*z* 463.73 (Table 1b).

The effect of the reaction time on the *N*′-hydroxyalkylation of the 1-hexadecyl-2-methyl imidazole has been studied. The reaction kinetics were followed by studying the disappearance of reactant peaks at 3.8 ppm for 1-hexadecyl-2-methyl imidazole and the appearance of a new methylene proton peak at 4.2 ppm for 1-hexadecyl-3-(10-hydroxydecyl)-2-methylimidazolium chloride. By using the ratio method of peak area integration, we quantified the amount of final compound formed. The peak at 0.9 ppm (proton peak corresponding to methyl group) was used to normalize the peak at 3.8 ppm and 4.2 ppm. Fig. 3 illustrates the percent conversion of starting compound and percent formation of final product at 110 °C. With extended reaction time, more conversion of reactant to product was observed. A conversion level of about 90% is obtained in 20 days using a stoichiometric amount of the reactants. The reaction was substantially complete before this time, but the product

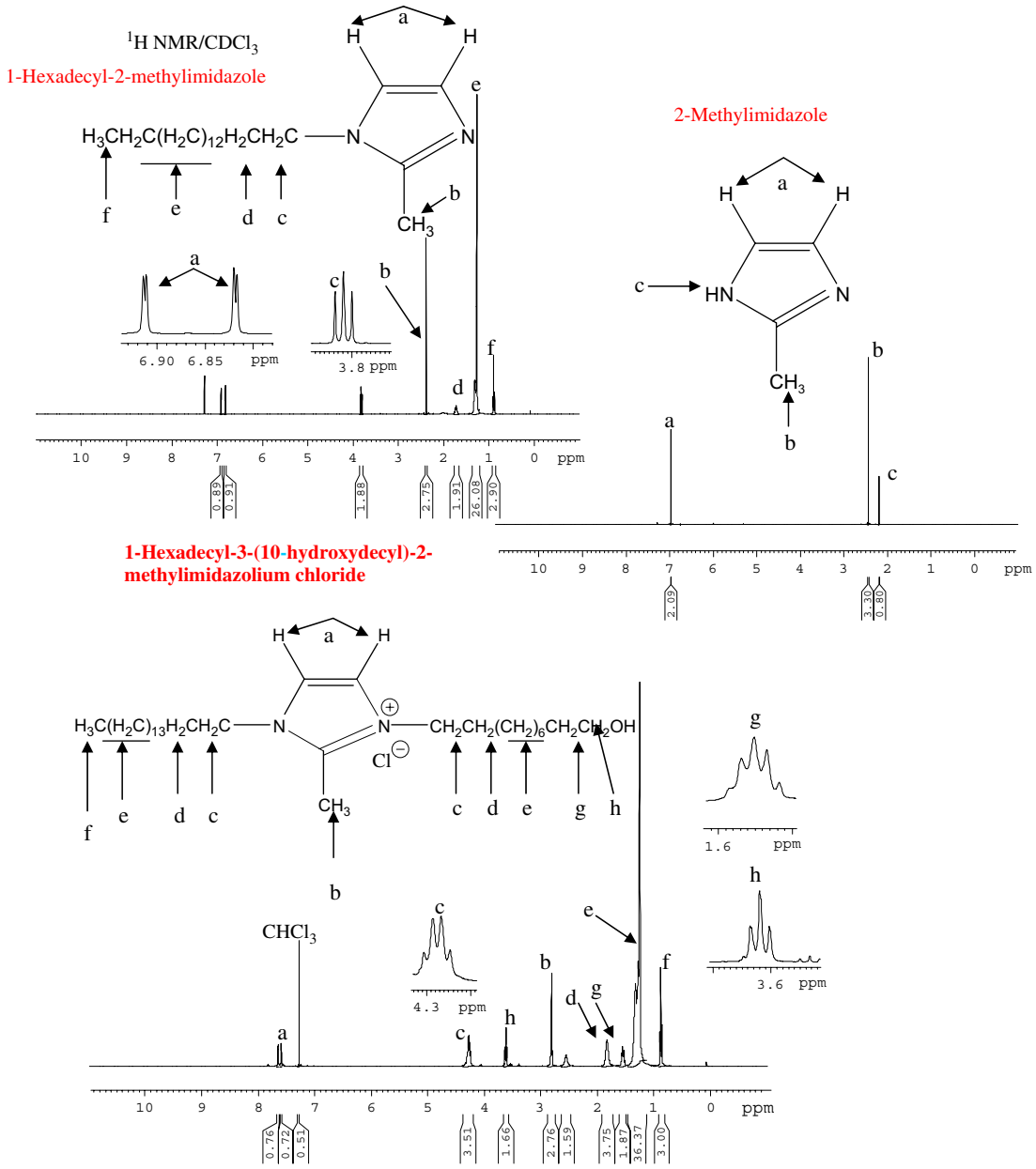

Fig. 2. NMR spectra of (a) 2-methyl imidazole, (b) 1-hexadecyl-2-methyl imidazole, and (c) 1-hexadecyl-3-(10-hydroxydecyl)-2-methylimidazolium chloride.

was stable to the reaction conditions, and the long reaction time allowed high conversion and isolation of the product in rather high purity directly from the reaction mixture.

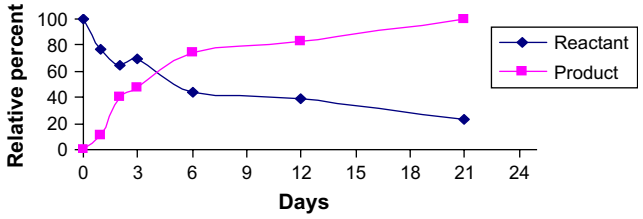

Fig. 3. Percent conversion of 1-hexadecyl-2-methyl imidazole to 1-hexadecyl-3-(10-hydroxydecyl)-2-methylimidazolium chloride with time.

The *N*-alkylation of 2-methyl imidazole and *N*′-hydroxyalkylation of *N*-alkylated 2-methyl imidazole can be extended to prepare other *N*,*N*′-substituted heterocycles, which could serve as ionomers in the functionalization of clay and formulation of high-temperature nanocomposite. Studies are underway to synthesize a homologous series of *N*,*N*′-substituted heterocycles for use in nanocomposites.

3.1. Characterization of imidazolium intercalated montmorillonite

The CEC of Na^+-montmorillonite (MMT) is reported to be 92.6 mmol/100 g [49]. Fig. 4 shows the TGA thermograms of HDMIM clay, and HDHDMIM clay. The TGA spectrum of

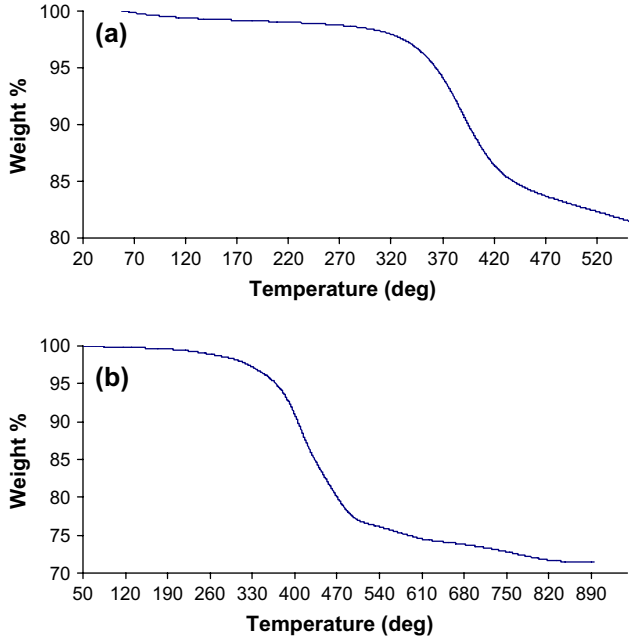

Fig. 4. TGA analysis of (a) Nile Blue-1-hexadecyl-2-methylimidazolium clay (NB-HDMIM-MMT) and (b) Nile Blue-1-hexadecyl-3-(10-hydroxydecyl)-2-methylimidazolium clay (NB-HDHDMIM-MMT).

HDMIM clay, and HDHDMIM clay has T_{dec} (5% weight loss) of 370 °C. As a point of reference, it is worthwhile to mention that the thermal decomposition of octadecyl ammonium salt from clay occurs at 210 °C (unpublished data). One of the interesting observations of this work is the increase in the onset temperature of decomposition of imidazolium intercalated montmorillonite clay. This result is very significant because it paves the way for formulating high-temperature matrix materials, such as bismaleimide, polyimide, high T_g epoxy resin in the formulation of fiber reinforced composites where organoclay filler can withstand high temperature. The use of imidazolium clays has been successfully employed in preparing clay thermoplastic nanocomposite with polyethylene terephthalate (processing temperature 300 °C) [36].

To establish that the imidazolium ions have indeed replaced gallery Na^+ ions on MMT, XRD of the organically modified clay was performed and compared with that of fully dried montmorillonite. The *d*-spacing of purified NB-HDMIM-MMT and NB-HDHDMIM-MT was found to be 1.83 ± 0.05 nm (2σ) and 2.20 ± 0.03 nm (2σ), respectively. Since the thickness of the silicate layer is 0.98 nm, the interlayer spacing after imidazolium treatment of NaMMT is 0.8 nm. As expected, the clay interlayer spacing increases with the long alkyl chain of the imidazolium salt on the clay surface. This is similar to the *d*-spacing for imidazolium-MMT reported previously [35].

3.2. Characterization of nanocomposite

Previous work has pointed out that different tools such as TEM and XRD may give a different picture of the state of clay platelet morphology in polymer matrices [50–54]. TEM and XRD provide essential information on the structure of the nanocomposite (interlayer distance of clay) with some limitations. Since TEM investigates only a small volume of the bulk material and is laborious, conclusions on the overall morphology of clay platelets in bulk should be viewed cautiously. Furthermore, the resolution and sensitivity of X-ray scattering may not be able to pick up the presence of a small-scale intercalation and/or agglomeration of clay in the polymer matrix. Therefore, these methods may be inconclusive in showing the state of exfoliation and dispersion of clay in bulk polymer matrix. Less labor intensive characterization methods that compliment TEM and XRD characterization of polymer nanocomposites, and that allow characterization over length scales in the micrometer to the submicrometer scale of the entire bulk sample would be desirable. Laser scanning confocal microscopy has been employed here as an alternative characterization tool to study clay dispersion in thermoset epoxy matrix. This is a bulk characterization tool and sample preparation is minimal. This approach has been useful in characterization of carbon nanotube polymer nanocomposite [55]. The level of clay dispersion in several epoxy nanocomposite specimens was compared and contrasted using TEM, XRD, and confocal microscopy techniques.

3.3. Hand mixed nanocomposite

After adding epoxy resin to organoclay clay (3.5 wt%), hand mixing the mixture, and curing the epoxy resin, a peak at $2\theta = 2.8^\circ$ corresponding to intercalated clay is observed along with the original peak (Fig. 5). The dark lines in the TEM micrograph (Fig. 6) of hand mixed NB-HDMIM-MMT epoxy nanocomposite correspond to MMT layers; this indicates a tactoid structure in the epoxy matrix. The clay has an average minimum layered stack thickness of 100 nm and corresponded to a minimum of 40 layers (Fig. 6a and b).

The role of diluent and high powered ultrasonication on clay dispersion in the epoxy matrix was evaluated. Before

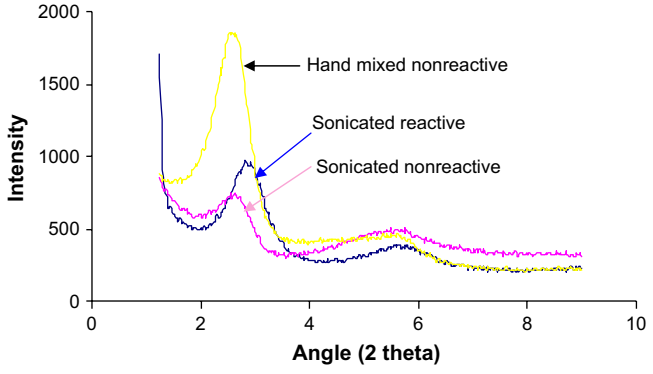

Fig. 5. Wide-angle X-ray diffraction of (a) hand mixed and (b) ultrasonication mixed NB-HDMIM-MMT epoxy nanocomposite and (c) ultrasonication mixed NB-HDHDMIM-MMT epoxy nanocomposite.

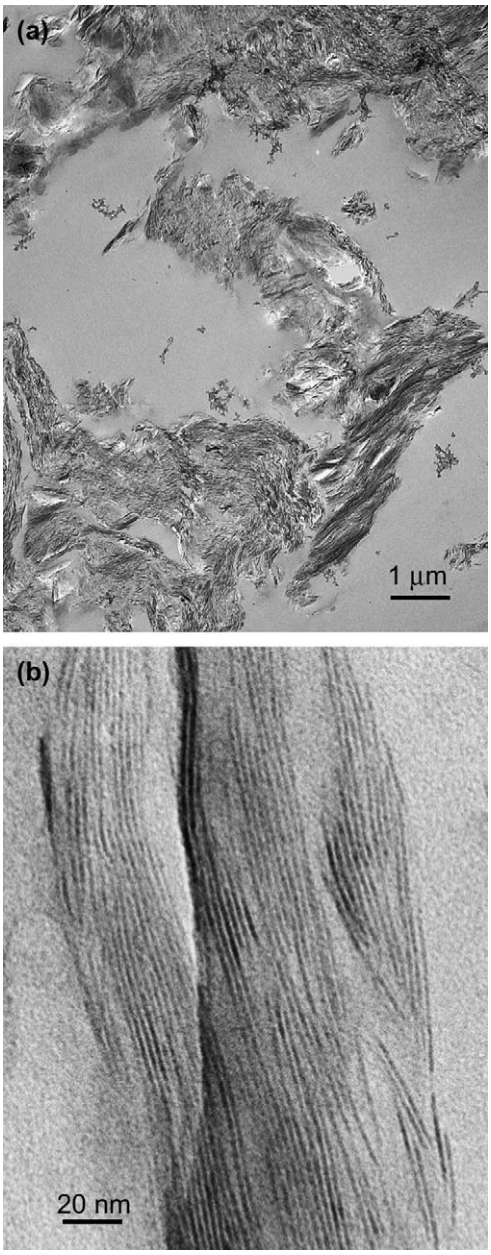

Fig. 6. TEM images of hand mixed NB-HDMIM-MMT epoxy nanocomposite samples. Part figures (a) and (b) are the low and high magnification images, respectively.

ultrasonication, the clay and resin were soaked separately in glycidyl methyl acrylate for several hours and then combined. At low magnification, the TEM images reveal that clay is better dispersed than the hand mixed samples (Fig. 7a). At higher magnification, all samples exhibit dispersion of stacks of MMT layers that range from 5 to 10 layers in size (Fig. 7b). The benefits of sonication in dispersing clay platelets in epoxy matrix are clearly noticeable. However, a word of caution that prolonged agitation of clay–resin mixture by rapid mixing technique may result in the molecular weight reduction of polymer and/or reduction in the aspect ratio of nanoclay platelets as well as possible thermal degradation of the clay surfactant [56]. Therefore, the usefulness of ultrasound sonication in achieving dispersion of nanoclay platelets in polymer matrix should be carefully studied against any compromise in the mechanical properties of the nanocomposite.

The XRD results are consistent with TEM observation, where the small tactoid (2–10 clay platelets) morphology was found in the sonicated sample. Unlike the hand mixed sample, the sonicated sample has shallow low angle peak at 2.8° that is considerably diffused (refer Fig. 5).

For deriving any quantitative information about clay platelet distribution, we estimated the platelet-neighboring platelet spacing. Our model assumes a regular, repeating lamellar structure of alternating clay and epoxy matrix. Fig. 8 is the histogram representation of clay platelet separation in the epoxy matrix as calculated from several TEM micrographs. The average platelet to platelet separation was found to be 4.5 nm, with some clay platelets having better separation. Generally, clay platelet separation like that described by the data in Fig. 8 is commonly referred to as a mixed intercalated-exfoliated morphology (Fig. 9).

An attempt was made to further improve clay platelet separation in the resin, by using hydroxyl functional organoclay (1-hexadecyl-3-(10-hydroxydecyl)-2-methylimidazolium-MMT) to form reactive clay. The epoxy and glycidyl resins along with clay were mixed using sonication. Low magnification TEM of the nanocomposite showed far fewer tactoids and stacks of MMT layers that range from 3 to 8 layers in number. The stacks of clay platelets are uniformly distributed in the epoxy matrix. The separation between neighboring clay platelets in reactive epoxy nanocomposite is better than that of the hand mixed samples, while the dispersion of the clay platelets in the reactive epoxy nanocomposite has been improved relative to that of nonreactive sonicated epoxy nanocomposite. The improved dispersion of clay in reactive nanocomposite is believed to be because of the presence of hydroxyl functionality in imidazolium salt. The hydroxyl group of the functionalized clay can assist in forming a strong chemical bond interface with the epoxy matrix. For example, specific associations between the functionalized clay and epoxy resin have been proposed in the formulation of epoxy nanocomposite. One can envision the formation of copolymer structures, homopolymer and the hybrid structures at the interface [57]. The characterization of the epoxy nanocomposite to establish the coupling of imidazolium treated clay, glycidyl methyl acrylate, and/or epoxy matrix resin is a difficult and complex issue and is a part of an on-going investigation.

Fluorescence labeling is one convenient method to follow resin curing and the clay delamination process in the monomer state, during curing and in the cured state [58,59]. Further characterization of the ‘‘ultrasonication mixed NB tagged HDMIM-MMT’’, ‘‘hand mixed NB tagged HDMIM-MMT’’ and ‘‘ultrasonication mixed NB tagged HDHDMIM-MMT’’ epoxy nanocomposite samples using laser scanning confocal microscopy is shown in Fig. 10. The two phase morphology is evident in confocal images, where the clay appears as bright images and epoxy matrix as dark regions. Nile Blue-tagged imidazolium functionalized clay particles in cured resin were studied by confocal laser microscopy. Nile Blue A is a cationic

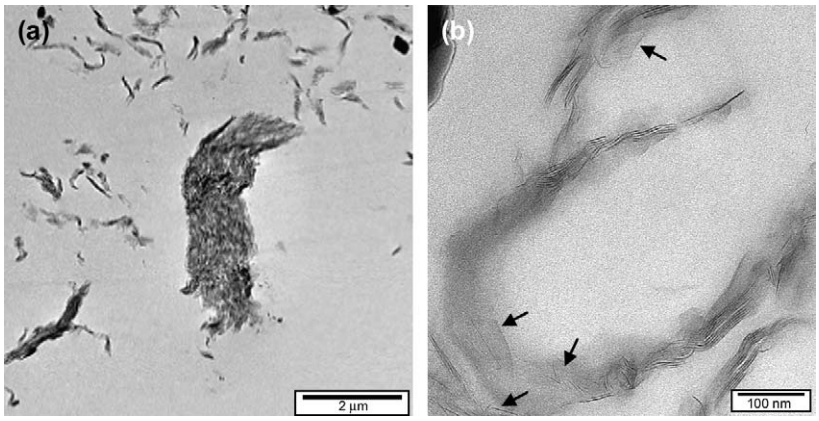

Fig. 7. TEM images of ultrasonication mixed NB-HDMIM-MMT epoxy nanocomposite samples. Part figures (a) and (b) are the low and high magnification images, respectively.

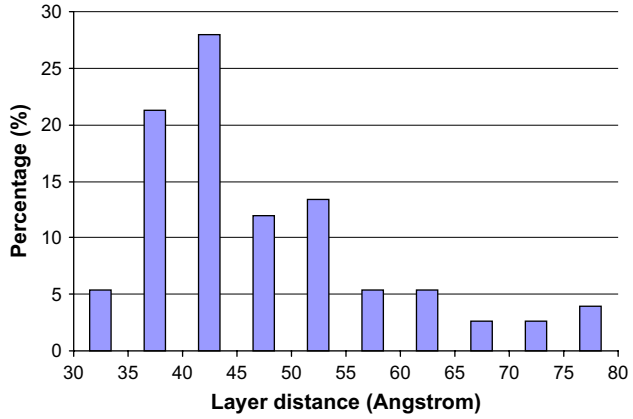

Fig. 8. Histogram representation of the distribution of clay platelet separation in an ultrasonication mixed NB-HDMIM-MMT epoxy nanocomposite sample.

probe, which intercalates into the clay via cation exchange [39]. Fig. 10a is of the hand mixed NB tagged HDMIM-MMT epoxy nanocomposite sample. Using a laser excitation wavelength of 488 nm, the Nile Blue-tagged HDMIM-MMT clay nanocomposite is observed for fluorescence emission at 560–615 nm. When the particle is poorly dispersed in the epoxy matrix, strong fluorescence emission is observed around the large clay particles (>10 μm).

However, when clay–epoxy mixture was mixed for 30 min by sonication, fluorescence emissions were noticed around smaller particles. Fig. 10b is the image of ''ultrasonication mixed NB tagged HDMIM-MMT'' epoxy nanocomposite sample. The intensity of the fluorescence emission was sufficient to detect the dispersion of clay (10–30 μm particles) in the epoxy matrix. Visual inspection of the confocal images confirms the relative better quality of clay dispersion in sonicated epoxy nanocomposite specimen relative to the hand mixed sample. Quantitative analysis of the images enables the three epoxy samples to be distinguished. Quantification was accomplished using intensity versus distance data taken along the horizontal line shown in each center-image. This gives a quantitative indication of the level of variation in the image. The mean intensity $(\bar{x})$ and the relative noise $(2\sigma/\bar{x})$ have been calculated

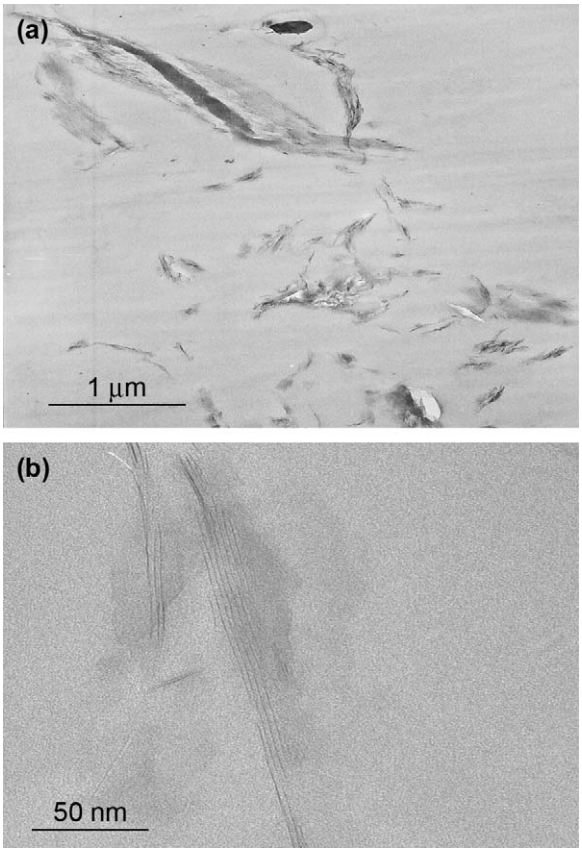

Fig. 9. TEM micrographs of ultrasonication mixed NB-HDHDMIM-MMT epoxy nanocomposite samples. Part figures (a) and (b) are the low and high magnification images, respectively.

along this line; the lower the relative noise the more homogeneous the sample. These data were averaged over 20 lines (taken every 20 μm) using a composite image made from 25 optical sections (taken every 1 μm). The quantitative analysis of the confocal data shows the benefit of ultrasonication for the two epoxy samples over the hand mixing protocol (see Fig. 10).

Finally, the confocal microscopy was used to study the distribution of clay platelets in reactive organoclay nanocomposite.

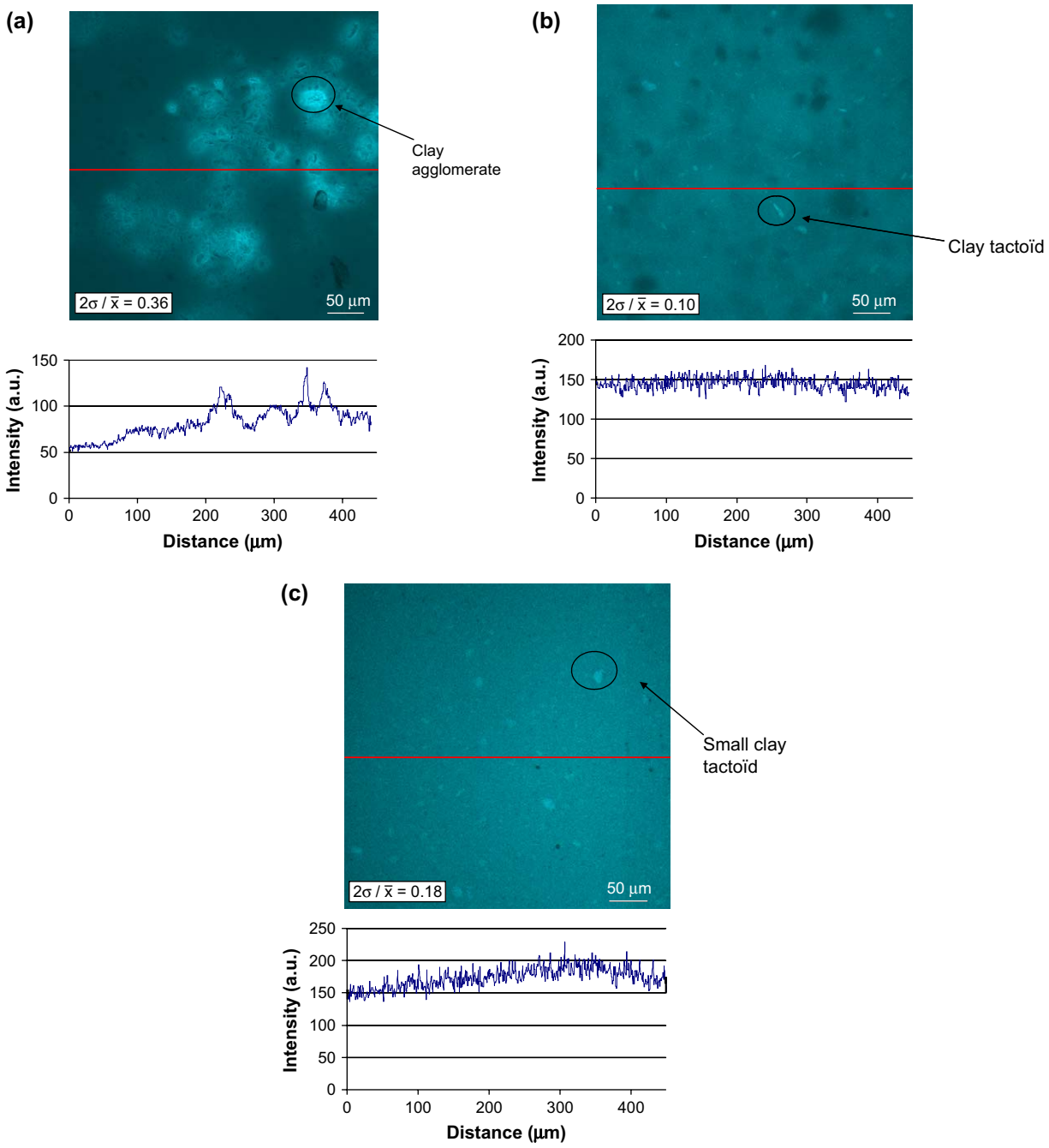

Fig. 10. Confocal image of epoxy samples. (a) Hand mixed NB tagged HDMIM-MMT nanocomposite sample, (b) ultrasonication mixed NB tagged HDMIM-MMT nanocomposite sample and (c) ultrasonication mixed NB tagged HDHDMIM-MMT nanocomposite sample. Intensity versus distance plot for the horizontal lines of each of the confocal image is shown.

The use of reactive organoclay HDHDMIM-MMT instead of HDMIM-MMT slightly improved the final morphology of nanocomposite. The relative noise $(2\sigma/\bar{x})$ of the confocal data for Fig. 10c and a was 0.18 and 0.36, respectively, suggesting a homogeneous distribution of the clay platelets in the sonicated reactive organoclay nanocomposite sample relative to the hand mixed sample. These results were similar in magnitude to that of sonication mixed nonreactive organoclay nanocomposite. Through these results, we demonstrate that the degree of exfoliation and dispersion of layered silicate nanocomposite are predominantly affected by processing and to a small degree by the clay chemical treatment.

The confocal results are in good agreement with TEM and XRD characterization results and allow characterization over several length scales ranging from the micrometer to the nanometer scale. In addition, the confocal analysis is 3–5 times faster than TEM analysis. This approach should be applicable to the characterization of other nanocomposites by using dye-tagged carbon nanotubes, nanosilicas, and polyhedral oligosilsesquioxanes (POSS).

4. Conclusions

The following conclusions can be drawn from the current work.

1. The starting compound 2-methyl imidazole was treated with sodium hydride and bromohexadecane to form 1-hexadecyl-2-methyl imidazole and the compound was protonated to form 1-hexadecyl-2-methylimidazolium chloride (HDMIM). The 1-hexadecyl-2-methyl imidazole was reacted with chlorodecanol in anhydrous acetonitrile to obtain 1-hexadecyl-3-(10-hydroxydecyl)-2-methylimidazolium chloride (HDHDMIM). The synthesized compound(s) were characterized by ^{1}H NMR and matrix assisted laser desorption/ionization time-of-flight mass spectrometry (MALDI-TOF MS).
2. Thermal stability of imidazolium functionalized clay (HDMIM-MMT and HDHDMIM-MMT) was found to be far superior to that of ammonium functionalized clay that is reported in the literature.
3. XRD and TEM results show that hand mixed nonreactive clay (HDMIM-MMT) epoxy nanocomposite exhibits tactoid morphology while ultrasonicated mixed nonreactive clay exhibits mixed morphology. A detailed study of the distribution of clay platelets and layer spacing in epoxy matrix indicates that on an average the interlayer spacing is 4.5 nm. TEM study of ultrasonication mixed reactive clay (HDHDMIM-MMT) epoxy nanocomposite exhibits highly dispersed clay platelets in epoxy matrix.
4. For the first time, confocal microscopy was used to obtain quantitative information of mesoscale dispersion of Nile Blue-tagged MMT platelets in cured epoxy matrix. There was evidence of aggregated clay platelet regions in the hand mixed sample. Sonication of the sample improved the separation of clay platelets and the combined effect of sonication as well as use of reactive clay gave well dispersed clay platelet distribution in epoxy nanocomposite. Visual inspection and image analysis of the confocal images confirmed the superior quality of the clay dispersion in sonicated samples as opposed to hand mixed nanocomposite samples. The positive attributes of confocal microscopy are that the clay platelet distribution throughout the bulk specimen can be obtained in 3 h with minimal sample preparation and is a non-destructive quantitative technique. TEM and X-ray diffraction support the conclusion that was observed from confocal microscopy.

Acknowledgments

This work was supported by the Air Force Office of Scientific Research under Grant # FA9550-04-1-0021, Grant # FA9550-06-1-0266, and NSF DMR-0213695. The authors thank M. Williams from NIST for assisting with the XRD measurements, L.P. Sung and M. Cicerone from NIST for providing LSCM facilities.

References

[1] Kojima Y, Usuki A, Kawasumi M, Okada A, Fukushima Y, Kurauchi T, et al. J Mater Res 1993;8:1185–9.
[2] Messersmith PB, Giannelis EP. J Polym Sci Polym Chem Ed 1995;33:1047–57.
[3] Kornmann X, Berglund LA, Sterte J, Giannelis EP. Polym Eng Sci 1998;38(8):1351–8.
[4] Wang Z, Pinnavaia TJ. Chem Mater 1998;10(12):3769–71.
[5] Shah AP, Gupta RK, Gangarao HVS, Powell CE. Polym Eng Sci 2002;42(9):1852–61.
[6] Giannelis EP. Adv Mater 1996;8(1):29–35.
[7] Vaia AR, Wagner HD. Mater Today 2004;7(11):32–7, 38–42.
[8] Lagaly G. Appl Clay Sci 1999;15:1–9.
[9] Ray SS, Okamoto M. Prog Polym Sci 2003;28(11):1539–641.
[10] Schmidt D, Shah D, Giannelis EP. Curr Opin Solid State Mater Sci 2002;6(3):205–12.
[11] Garces JM, Moll DJ, Bicerano J, Fibiger R, McLeod DG. Adv Mater 2000;12:1835–9.
[12] Liu W, Hoa SV, Pugh M. Compos Sci Technol 2005;65(2):307–16.
[13] Park J, Jana SC. Polymer 2004;45(22):7673–9.
[14] Barker O, Varley RJ, Simon PG. Eur Polym J 2004;40(1):187–95.
[15] Chen C, Khobaib M, Curliss D. Prog Org Coat 2003;47(3–4):376–83.
[16] Tolle TB, Anderson PD. Compos Sci Technol 2002;62(7–8):1033–41.
[17] Chin I, Thurn-Albrecht T, Kim H, Russell PT, Wang J. Polymer 2001;42(13):5947–52.
[18] Kornmann X, Lindberg H, Berglund A. Polymer 2001;42(10):4493–9.
[19] Tsai J, Sun CT. J Compos Mater 2004;38(7):567–79.
[20] Brown JM, Curliss D, Vaia RA. Chem Mater 2000;12:3376–84.
[21] Zilg C, Thomann R, Baumert M, Finter J, Mulhaupt. Macromol Rapid Commun 2000;21(17):1214–9.
[22] Ishida H, Campbell S, Blackwell J. Chem Mater 2000;12:1260–7.
[23] Fu XA, Qutubuddin S. J Colloid Interface Sci 2005;283(2):373–9.
[24] Yebassa D, Balakrishnan S, Feresenbet E, Raghavan D, Start PR, Hudson SD. J Polym Sci Polym Chem Ed 2004;42:1310–9.
[25] Bourbigot S, Vanderhart DL, Gilman JW, Bellayer S, Stretz H, Paul DR. Polymer 2004;45:7627–38.
[26] Zhen X, Wilkie CA. Polym Degrad Stab 2003;81:539–50.
[27] Becker O, Cheng Y-B, Varley RJ, Simon GP. Macromolecules 2003;36:1616–25.
[28] Zhu J, Uhl MF, Morgan BA, Wilkie AC. Chem Mater 2001;13:4649–54.
[29] Xie W, Gao Z, Pan W-P, Hunter D, Singh A, Vaia R. Chem Mater 2001;13:2979–90.
[30] Davis RD, Gilman JW, Sutto TE, Callahan JH, Trulove PC, Delong HC. Clays Miner 2004;52(2):171–7.
[31] Lan T, Kaviratna PD, Pinnavaia JT. J Phys Chem Solids 1996;57:1005.
[32] Wang SM, Pinnavaia JT. Chem Mater 1994;6:468–74.
[33] Sue HJ, Gam TK, Bestaoui N, Clearfield A, Miyamoto M, Miyatake N. Acta Mater 2004;52(8):2239–50.
[34] Severe G, Hsieh JA, Koene EB. In: 58th ANTEC, vol. 2; 2000. p. 1523–6.
[35] Gilman JW, Awad WH, Davis RD, Sheilds J, Harris Jr RH, Davis C, et al. Chem Mater 2002;14:3776–85.
[36] Davis CH, Mathias LJ, Gilman JW, Schiraldi JR, Trulove P, Sutto TE, et al. J Polym Sci Polym Phys 2002;40(23):2661–6.
[37] Ngo H, LeCompte K, Hargens L, McEwen BA. Thermochim Acta 2000;357:97–105.
[38] Begg G, Grimmett RM, Wethey DP. Aust J Chem 1977;30:2005–15.
[39] Maupin PH, Gilman JW, Bourbigot S, Harris Jr RH, Bellayer S, Bur AJ, et al. Macromol Rapid Commun 2004;25(7):788–92.
[40] Gilman Sr J, Davis RD, Bellayer S, Maupin PH, Raghavan D, Langat J, et al. In: Proceedings of the American chemical society, vol. 92. Division of Polymeric Materials: Science and Engineering; 2005. p. 168–70.
[41] Xie W, Xie R, Pan W, Hunter D, Koene Bryan, Tan L, et al. Chem Mater 2002;14:4837–45.
[42] Wang ZM, Chung TC, Gilman JW, Manias E. J Polym Sci Part B 2003;41:3173–87.

[43] Bottino FA, Fabbri E, Fragala IL, Malandrino G, Orestano A, Pilati F, et al. Macromol Rapid Commun 2003;24:1079–84.
[44] Kornmann X, Thomann R, Finter J, Berglund LA. Polym Eng Sci 2002;42:1815–22.
[45] Lopez-Pestana JM, Diaz-Teran J, Avila-Rey JM, Rojas-Cervantes LM, Martin-Aranda MR. Microporous Mesoporous Mater 2004;67:87–94.
[46] Khabnadideh S, Rezaei Z, Khalafi-Nezhad A, Bahrinajafi R, Mohamadi R, Farrokhroz AA. Bioorg Med Chem Lett 2003;13(17): 2863–6.
[47] Awad WH, Gilman JW, Nyden M, Harris Jr RH, Sotto TE, Callahan J, et al. Thermochim Acta 2004;409:3–11.
[48] Reddy GS, Hobgood Jr RT, Goldstein JH. J Am Chem Soc 1962;84: 336–40.
[49] Song M, Wong CW, Jin J. Polym Int 2005;54:560–8.
[50] Chu L-L, Anderson SK, Harris JD, Beach MW, Morgan AB. Polymer 2004;45(12):4051–61.
[51] Morgan AB, Gilman JW, Jackson CL. Macromolecules 2001;34:2735–42.
[52] Morgan AB, Gilman JW. Appl Polym 2003;87:1329–38.
[53] Perrin-Sarazin F, Ton-That MT, Bureau MN, Denault J. Polymer 2005;46:11624–34.
[54] Vermogen A, Masenelli-Varlot K, Seguela R, Duchet-Rumeau J, Boucard S, Prele P. Macromolecule 2005;38:9661–9.
[55] Bellayer S, Gilman JW, Eidelman N, Bourbigot S, Flambard X, Fox DM, et al. Adv Funct Mater 2005;15:910–6.
[56] Dennis HR, Hunter DL, Chang D, Kim S, White S, White JL, et al. Polymer 2001;42:9513–22.
[57] Kornmann X, Lindberg H, Berglund L. Polymer 2001;42:4493–9.
[58] Eidelman N, Raghavan D, Forster AM, Amis EJ, Karim A. Macromol Rapid Commun 2001;25:259–64.
[59] Yoonessi M, Toghiani H, Kingery LW, Pittman Jr UC. Macromolecules 2004;37(7):2511–8.